*FUDMA Journal of Sciences (FJS)*
*ISSN online: 2616-1370*
*ISSN print: 2645 - 2944*
*Vol. 10 No. 16, June, 2026, pp 594 – 606*
*DOI:* https://doi.org/10.33003/fjs-2026-1016-5916

# Evaluation of the Phase Hydrolysis of Crude Red Oil Filtrate-Based Electrolytes Formulated with Sodium Chloride (NaCl) And Potassium Chloride (KCl) Salts for Battery Applications

**[1]M. Alpha, [1]A.Y. Jamila, [1]A.Z. Ngari, [2]M, Jemimah, [3]Y.S. Sanda, and [1]M. Mujaheed**

[1]Nigerian Army University, Biu, Borno State, Nigeria.
[2]Kaduna State University, Kaduna State, Nigeria.
[3]National Agency for Science and Engineering Infrastructure, FCT Abuja, Nigeria.

*Corresponding authors' email: alphamatthew4@gmail.com

**Received:** 17 Aug. 2026
**Accepted:** 24 Aug. 2026
**Published:** 08 Sep. 2026

**ABSTRACT**
Developing sustainable, non-toxic electrolytes from biomass faces challenges due to low salt dissociation and poor ion mobility in hydrophobic lipid environments. This study presents a comprehensive structural analysis of green liquid-matrix electrolytes composed of red palm oil (RPO) mixed with alkali chloride salts (NaCl or KCl) and distilled water. Using Fourier Transform Infrared (FTIR) spectroscopy, we systematically evaluate twelve formulation variations (Samples A to L) to establish relationships between structural configuration and potential battery performance. Attenuated Total Reflection (ATR-FTIR) monitoring revealed a notable coordinate bathochromic shift of the triglyceride ester carbonyl to 1737.92 $cm^{-1}$ uniquely in the NaCl system (Sample A), indicating direct cation chelation. Conversely, the KCl system maintained a baseline ester peak at 1743.71 $cm^{-1}$, indicating that larger $K^+$ ions remain confined within polar aqueous microchannels. Furthermore, critical boundaries were identified between water-overloaded systems displaying extensive hydrogen bonding (3394.83 $cm^{-1}$) and oil-encapsulated micellar networks. Spectroscopic evidence also uncovered an identical partial hydrolysis pathway for both salts (1712.85 $cm^{-1}$ free fatty acid shoulder), highlighting a key challenge for battery shelf-life. Finally, a comparison of methods showed that classical KBr pelletization causes phase displacement that obscures organic signatures, establishing ATR as the required technique for characterisation. These findings provide a framework for balancing ionic conductivity, voltage stability, and corrosion resistance in biomass-derived liquid batteries.

**Keywords:** Red palm oil, Liquid matrix electrolyte, Batteries, ATR-FTIR, Phase hydrolysis

## INTRODUCTION

The escalating global energy crisis and environmental degradation associated with fossil fuels have accelerated the search for sustainable, "green" energy storage systems. Central to this transition is the development of electrolytes that are non-toxic, biodegradable, and cost-effective. Traditional electrolytes in lithium-ion batteries and supercapacitors often rely on synthetic polymers and organic solvents that pose significant recycling challenges and environmental hazards (Alpha et al., 2019; Smith et al., 2021; Bard and Faulkner, 2014). Consequently, bio-based materials, specifically vegetable oils, have emerged as promising candidates for electrolyte host matrices due to their abundance and inherent dielectric properties.

Red palm oil filtrate is unique among vegetable oils due to its high concentration of phytonutrients, including carotenoids and tocotrienols. Beyond its nutritional value, its chemical structure, comprising a mixture of saturated and unsaturated fatty acids, provides a viscous medium capable of suspending ionic species (Okonkwo and Mensah, 2022; Borghols et al., 2009). Previous studies indicate that the antioxidant profile of red oil can enhance the oxidative stability of electrochemical systems, protecting the electrolyte from premature chemical breakdown during cycling (Yusuf et al., 2023; Chen et al, 2006; Chen et al., 2019). However, oil is naturally an insulator; its utility in electrochemistry depends entirely on the successful integration of conductive salts.

At the macro-level, the performance of the mixture is defined by its ionic conductivity (σ). This is derived from Ohm's Law, where the resistance (R) encountered by the current is inversely proportional to the conductivity:

$$\sigma = L/(R.A) \quad (1)$$

In this research, L represents the distance between electrodes and A the surface area. For a bio-electrolyte to be viable, it must minimize bulk resistance (R) to ensure efficient energy transfer.

The most critical constraint in this study is the relationship between the electrolyte's molar conductivity (ʌ) and the solvent's viscosity (η), known as Walden's Rule:

$$ʌη = \text{constant} \quad (2)$$

Red oil filtrate possesses a significantly higher viscosity than water or acetonitrile. According to Walden's Rule, this high viscosity imposes a "frictional drag" on the ions, which suggests that the molar conductivity of the mixture will be inherently lower than that of aqueous electrolytes (Chen and Zhang, 2020). The research must therefore determine if the chemical benefits of red oil outweigh this physical limitation.

To compare the efficiency of Na+ versus K+ ions, we apply the Stokes-Einstein Relation. This formula calculates the diffusion coefficient (D) of an ion based on its radius (r):

$$D = (K\_B\ T)/6\pi\eta r \quad (3)$$

(Yusuf et al., 2023).

There is a growing demand for sustainable, low-cost, and non-toxic electrolytes for electrochemical applications (such as batteries or sensors). Ideally, bio-based materials like crude red oil filtrate could serve as an effective host matrix when combined with abundant salts like sodium chloride (NaCl) to create 'green' energy solutions.

However, red oil is naturally a dielectric insulator with high viscosity, which typically hinders ionic mobility. While NaCl and KCl can introduce conductivity, the specific interaction between the complex organic compounds in crude red oil (like carotenes and fatty acids) and the inorganic ions of NaCl and KCL are not well understood.

Currently, there is a lack of data regarding the optimal mixing ratio and the electrochemical stability of this specific mixture. Without characterizing its ionic conductivity and stability window, it remains unknown whether this bio-mixture can realistically replace synthetic, toxic electrolytes in practical devices (Kato et al., 2022; Nadeen et al., 2023)

While bio-based crude red oil filtrate is a promising medium for green electrolytes, its performance is highly dependent on the choice of salt used to provide ionic conductivity. Current literature lacks a comparative analysis of how the different ionic radii and binding affinities of Sodium Chloride (NaCl) and Potassium Chloride (KCl) specifically affect the charge transport efficiency, ionic conductivity, and chemical stability of the oil-salt mixture. This study aimed to fill that gap by identifying which salt provides the best balance between high ionic mobility and long-term resistance to lipid oxidation

This study is significant because it moves beyond 'proving a concept' to optimizing it. By comparing NaCl and KCl, the research will identify a superior bio-electrolyte recipe that maximizes power output while minimizing the chemical degradation of the oil host matrix. This research offers a scientific foundation for building low-cost, high-efficiency bio-batteries systems, and a non-toxic alternative to synthetic electrolytes. The findings provided crucial data for the engineering of 'green' batteries and supercapacitors, supporting global efforts toward environmental sustainability while providing an economic use-case for palm oil derivatives in the high-tech sector.

## MATERIALS AND METHODS

The crude red palm oil was first heated to 50 °C to ensure a completely liquid state. It was subsequently filtered using a vacuum filtration system equipped with a 0.45 µm membrane filter to remove any residual fibres or solid particulates. A 100 ml aliquot of the filtrate was then mixed with 50 mL of ethanol solvent (in a 2:1 oil-to-ethanol ratio). The mixture was dehydrated in a vacuum oven at 70 °C for 2 hours with continuous stirring at 500 rpm to eliminate trace moisture and residual ethanol, both of which could interfere with subsequent salt incorporation.

To facilitate the integration of NaCl and KCl salts into the oil phase, concentrated aqueous pre-mix solutions were prepared. For the single-salt systems, specific quantities of NaCl (2 g, 5 g, and 10 g) and KCl (2 g, 5 g, and 10 g) were each dissolved separately in 40 ml of deionized water and 40 ml of red palm oil, to obtain saturated electrolytes solutions, sample A (40 ml RPO + 40 ml deionized water from 2 g NaCl), sample B (40 ml RPO + 40 ml deionized water from 5 g NaCl), sample C (40 ml RPO + 40 ml deionized water from 10 g NaCl, sample D (40 ml RPO + 40 ml deionized water from 2 g KCl, sample E (40 ml RPO + 40 ml deionized water from 5 g KCl) and sample F (40 ml RPO + 40 ml deionized water from 10 g KCl). Also, a fixed mass of 2 g of NaCl, and 40ml of deionized water were dissolved in 10 ml, 20 ml, and 30 ml of red palm oil respectively, to obtain a mixture of an emulsion. the same procedure as above were applied for the KCl salt, to obtained an electrolyte solutions, samples G (5 g NaCl, 10 ml RPO, 40 ml deionize H2O), sample H (5 g NaCl, 20 ml RPO, 40 ml deionize H2O), sample I (5 g NaCl, 30 ml RPO, 40 ml deionize H2O), sample J (5 g KCl, 10 ml RPO, 40 ml deionize H2O), sample K (5 g KCl, 20 ml RPO, 40 ml deionize H2O) and sample L (5 g KCl, 30 ml RPO, 40 ml deionize H2O).

The electrolytes mixtures were heated to a constant temperature of 50 °C and stirred magnetically at 500 rpm for 30 minutes to enhance complete mixing. This process dispersed the aqueous salt solution into micro-droplets, thereby forming a stable water-in-oil emulsion. The electrolyte emulsions were then allowed to cool and were stirred at room temperature for an additional 30 minutes to facilitate stabilization. Finally, the mixtures were centrifuged for 30 minutes. The electrolyte system was considered stable when no visible phase separation (i.e., distinct oil and water layers) was observed after centrifugation.

## RESULTS AND DISCUSSION

### Discussion on effect of Viscosity on Electrolyte Samples

The overall electrochemical process introduced the effect of the viscosity of a three-phase emulsion system (Water, Oil, and Salt/Electrolytes). Since oil and water do not naturally mix, these formulations create an emulsion where salt ions concentrate in the water phase and at the oil-water interface, overwhelmingly affecting droplet stability, packing, and overall fluid friction. Table 1 and table 2 gives the results of the viscosity for the various samples.

**Table 1: Viscosity as a Result Of Variation of Salt in the Electrolyte Sample**

| Salt Mass in g | Viscosity µ ($mm^2/s$)/Samples | Viscosity µ ($mm^2/s$)/Samples |
|---|---|---|
| 2 | 6.40/A | 2.40/D |
| 5 | 4.85/B | 4.10/E |
| 10 | 3.20/C | 3.90/F |

**Table 2: Viscosity as a Result Variation of Red Palm Oil in the Electrolyte Sample**

| RPO Volume in ml | Viscosity µ ($mm^2/s$)/Samples | Viscosity µ ($mm^2/s$)/Samples |
|---|---|---|
| 10 | 1.50/G | 3.88/J |
| 20 | 4.35/H | 2.85/K |
| 30 | 4.12/I | 2.42/L |

***The Role of Salt Concentration (Mass of Salt)***

In oil-in-water or water-in-oil emulsions, it is important to know that salts modify the electrical double layer around droplets, driving either droplet aggregation (flocculation) or phase inversion. Viscosity changes with changes in salt mass in 40 ml RPO + 40 ml deionized water from 2 g NaCl (µ = 6.4 mm2/s) to 5 g NaCl (µ = 4.85 mm2/s) to 10 g NaCl (µ = 3.20 mm2/s). Also 2 g KCl (µ = 2.4 mm2/s) to 5 g KCl (µ = 4.10 mm2/s) to 10 g KCl (µ = 3.90 mm2/s).

Increasing NaCl from 2 g to 10 g causes viscosity to drop rapidly (6.40 mm2/s to 4.85 mm2/s to 3.20 mm2/s). At 2 g NaCl, the ions optimise the electrostatic repulsion and the

interfacial tension, keeping the red palm oil droplets firmly dispersed in a firm, highly viscous emulsion network. As more NaCl was added, (5 g to 10 g), the high concentration of Na+ ions shades the surface charges around the oil droplets matrix. This causes coalescence, the oil droplets merge into larger pockets, reducing the overall interfacial surface area and drastically thinning the mixture.

Increasing KCl causes viscosity to jump up at 5 g (μ = 2.40 mm2/s to μ = 4.10 mm2/s) before stabilising at 10 g (μ = 3.90 mm2/s). Potassium (K+) is a larger ion with lower charge density. At 2 g, it does not provide enough charge to stabilise a thick emulsion, leading to a weak, runny mixture. At 5 g, it reaches an optimal stabilisation zone where it bridges the interfacial layer, creating a uniform, stable, and thicker emulsion. Past 5 g, the system hits a saturation limit, keeping the viscosity relatively steady.

The physical differences between Sodium and Potassium heavily impact how they interact with the polar heads of the fatty acids naturally present in red palm oil (like palmitic and oleic acids). At 2 g Salt, NaCl (μ = 6.40 mm2/s) is much more effective at building a viscous emulsion than KCl (2.40 mm2/s). The smaller, highly hydrated Na+ bonds water molecules tightly at the oil interface, maximizing hydrodynamic resistance. At 10 g Salt: KCl (μ = 3.90 mm2/s) maintains a more stable viscosity than NaCl (3.20 mm2/s). Excess K+ ion resists over-screening, preventing severe phase separation at high salt levels.

**Discussion on Fourier Transform Infrared Spectroscopy (FTIR) of Electrolyte Samples**

The Fourier Transform Infrared Spectroscopy (FTIR) spectrum for sample A, analysed using Attenuated Total Reflection (ATR), shown in figure 1, illustrates the chemical profile of red palm oil mixed with sodium chloride (NaCl) and distilled water for a liquid-matrix battery application. This spectrum confirms a successful emulsion system where the fundamental triglyceride structure of the palm oil coexists alongside the aqueous electrolyte phase without undergoing extensive structural degradation. The Spectral analysis and functional groups for the sample is seen in table 3.

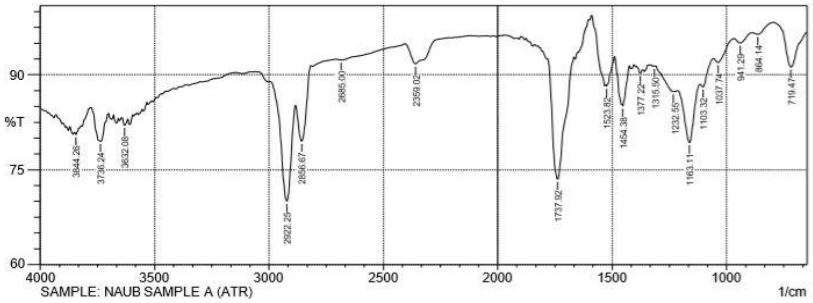


Figure 1: FTIR Spectra for Sample A

**Table 3: Spectral Analysis and Functional Groups for Sample A**

| Wavenumber ($cm^{-1}$) | Functional Group Assignment | Chemical Significance in Battery Application |
|---|---|---|
| 3844.26, 3736.24, 3632.08 | Sharp, multi-peaked free O–H stretching | Confirms the presence of uncoordinated and hydrogen-bonded water molecules serving as the primary salt-solvating medium. |
| 2922.25 & 2856.67 | Highly intense asymmetric and symmetric C–H stretching | Proves that the long, hydrophobic aliphatic hydrocarbon chains of the palm oil triglycerides remain fully intact. |
| 2685.00 & 2359.02 | Weak combination bands / environmental atmospheric $CO_2$ | Indicates standard background ambient atmospheric readings during testing. |
| 1737.92 | Extremely sharp, intense C=O (Carbonyl) stretching | Confirms the preservation of triglyceride ester bonds. The shift down to 1737 $cm^{-1}$ suggests strong coordination with the electrolyte. |
| 1523.82 | Carboxylate salt stretching / Shifted carbonyl complexation | Points to localized ion-dipole or chemical interactions between the dissolved $Na^+$ ions, water, and fatty acid groups. |
| 1454.38, 1377.22, 1315.50 | Aliphatic C–H bending (scissoring/rocking) | Validates the mechanical and structural stability of the underlying alkane fatty acid chains. |
| 1163.11, 1103.32, 1037.74 | C–O stretching vibrations of ester groups | Fingerprint region confirming that the core glycerol-fatty acid ester linkages have not collapsed. |
| 941.29 & 864.14 | Out-of-plane C=C-H bending or alkene variations | Represents unsaturated fatty acid configurations (like oleic or linoleic components) in the oil. |

A crucial indicator in this spectrum is the location of the ester carbonyl peak at 1737.92 $cm^{-1}$. The shift down to 1737 $cm^{-1}$ provides clear evidence of ion-dipole interaction. The smaller, highly charge-dense $Na^+$ ions from the dissolved NaCl are interacting with the lone electron pairs on the carbonyl oxygens, shifting the bond frequency downward

Pure palm oil possesses a low dielectric constant, rendering it incapable of effectively dissociating NaCl on its own. By incorporating distilled water (evident in the 3800–3600 $cm^{-1}$ range), the NaCl completely dissolves into free, highly mobile $Na^+$ and $Cl^-$ ions. In this liquid matrix setup, water acts as the high-dielectric transport medium to maximize initial ionic conductivity, while the viscous palm oil matrix stabilizes the blend and prevents rapid evaporation of the water phase.

The distinct peak at 1523.82 $cm^{-1}$ represents the creation of localized carboxylate coordination states. While water can theoretically catalyze the hydrolysis of triglycerides into free

fatty acids, the retention of a sharp, powerful 1737 $cm^{-1}$ peak proves that the bulk oil phase remains structurally intact. The 1523 $cm^{-1}$ peak implies a stable interfacial junction where the dissolved salt ions bridge the boundary between the hydrophobic oil and the hydrophilic aqueous phase.

Because this liquid matrix explicitly contains free water molecules, the operational voltage window of the battery cell will be controlled by the thermodynamic breakdown of water. To prevent water electrolysis (which triggers gas evolution, cell swelling, and electrode degradation), the charging voltage must be strictly regulated below 1.23 V.

The FTIR spectrum for sample B, as seen in figure 2, reveals a significantly higher water content and distinct phase changes within the liquid matrix. The spectrum shows an expanded, much broader hydroxyl footprint that fundamentally alters the local coordination network of the battery electrolyte. The Spectral analysis and functional groups for this sample is seen in table 4.

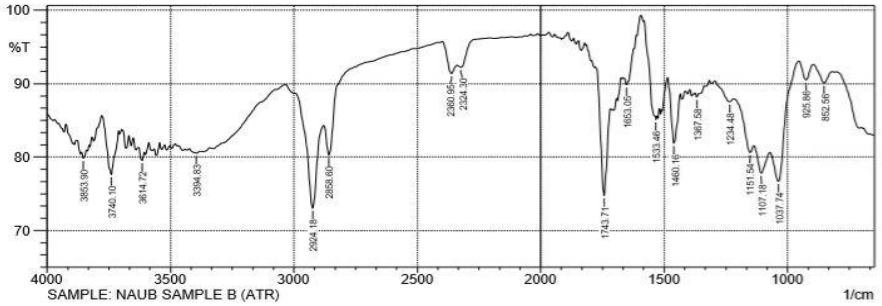


Figure 2: FTIR Spectra for Sample B

**Table 4: Spectral Analysis and Functional Groups for Sample B**

| Wavenumber ($cm^{-1}$) | Functional Group Assignment | Chemical Significance in Battery Application |
|---|---|---|
| 3853.90 to 3614.72 | Sharp, multi-peaked free O–H stretching | Represents uncoordinated, free water molecules responsible for dissolving the NaCl salt. |
| 3394.83 | Broad, deep hydrogen-bonded O–H band | Direct evidence of a highly dense network of hydrogen-bonded bulk water molecules surrounding the oil phases. |
| 2924.18 & 2858.60 | Aliphatic asymmetric & symmetric C–H stretching | Confirms that the hydrophobic triglyceride core of the red palm oil remains chemically stable. |
| 2360.95 & 2324.30 | Doublet from environmental atmospheric $CO_2$ | Standard ambient background reading during testing. |
| 1743.71 | Sharp C=O (Carbonyl) stretching | Confirms that the bulk ester linkages remain intact, centering back at 1743 $cm^{-1}$. |
| 1653.06 | H–O–H bending / C=C alkene stretching | Strong overlapping signals from the water phase and unsaturated fatty acids. |
| 1533.46 | Carboxylate salt or shifted carbonyl coordination | Points to interfacial ion coordination balancing the oil and water boundaries. |
| 1460.16 & 1367.58 | Aliphatic C–H bending configurations | Validates physical backbone stability within the lipid fatty acid profile. |
| 1234.48 to 1037.74 | Multi-peaked C–O stretching footprint | Represents the ester and glycerol skeletal linkages of the oil matrix. |

The defining signature of Sample B is the prominent valley centered at 3394.83 $cm^{-1}$. This broad band represents extensive hydrogen-bonded water molecules. In the liquid matrix battery setup, this indicates that Sample B has a much higher water-to-oil volume ratio. The water phase is not merely floating as trapped droplets; it has established a continuous bulk liquid network throughout the emulsion. Because the hydrogen-bonded water network is highly developed, the NaCl salt is completely dissociated into free sodium ($Na^+$) and chloride ($Cl^-$) ions. In terms of electrochemical transport, Sample B will likely exhibit the highest initial ionic conductivity. The free ions face lower resistance moving through the bulk aqueous microchannels compared to navigating the viscous oil matrix. Interestingly, the carbonyl ester peak centers at 1743.71 $cm^{-1}$ in this sample, returning to its baseline position. This suggests that because there is so much water present, the $Na^+$ are preferentially solvated by water molecules rather than coordinating tightly with the oil's carbonyl oxygens. The oil acts more as a physical stabilizer/thickener rather than a chemical chelator in this specific formulation. While the increased water content maximizes conductivity, it exacerbates the liquid cell's vulnerabilities. A broad water band at 3394 $cm^{-1}$ often correlates with weak emulsion stability. Over time, gravity will likely cause this mixture to phase-separate into distinct oil and water layers, which would instantly destabilize the battery's internal resistance.

The FTIR spectrum for sample C, as seen in figure 3, represents a red palm oil mixture with NaCl and distilled water for a liquid-matrix battery application. It shows a minimized water signature, representing a well-homogenized or heavily oil-dominated system where moisture is tightly restricted. The Spectral analysis and functional groups for this sample is seen in table 5

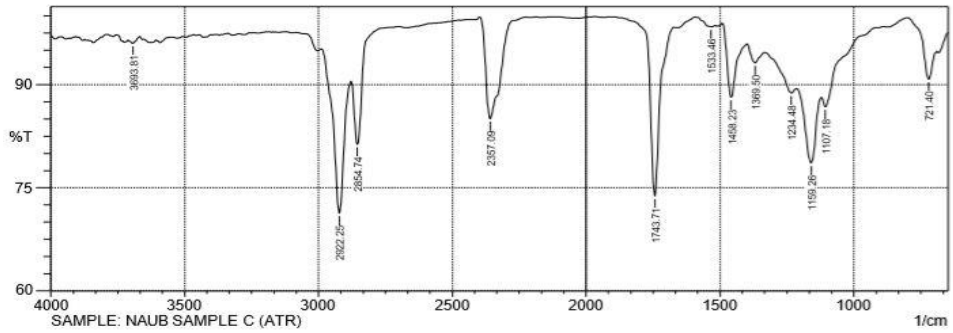


Figure 3: FTIR Spectra for Sample C

**Table 5: Spectral Analysis and Functional Groups for Sample C**

| Wavenumber ($cm^{-1}$) | Functional Group Assignment | Chemical Significance in Battery Application |
|---|---|---|
| 3693.81 | Isolated, weak free O–H stretch | Shows a highly restricted, trace presence of unbonded water molecules compared to Sample B. |
| 2922.25 & 2854.74 | Strong asymmetric & symmetric C–H stretching | Confirms the hydrophobic triglyceride core of the red palm oil remains robustly intact. |
| 2357.09 | Deep, sharp environmental atmospheric $CO_2$ | Represents standard background gas absorption during the testing cycle. |
| 1743.71 | Highly intense, sharp C=O (Carbonyl) stretching | Confirms pristine ester bonds. The baseline position suggests minimized direct coordination with free $Na^+$ ions. |
| 1533.46 | Extremely weak interfacial carboxylate peak | Indicates that phase boundaries or salt complexation are significantly reduced in this window. |
| 1458.23 & 1369.50 | Aliphatic C–H bending vibrations | Confirms mechanical and structural stability of the underlying alkane chains. |
| 1234.48, 1159.26, 1107.18 | Clean, distinct C–O stretching footprint | Represents the ester and glycerol skeletal linkages of the unhydrolyzed oil matrix. |
| 721.40 | Aliphatic $CH_2$\ rocking vibration | Proves the long hydrocarbon chains are well-preserved, dictating fluid viscosity. |

The most critical finding in Sample C is the near-complete absence of the broad hydrogen-bonded water band around 3400 $cm^{-1}$. Only a tiny, isolated peak at 3693.81 $cm^{-1}$ remains. This indicates that Sample C either contains a very low volume ratio of distilled water, or the formulation has successfully encapsulated the water inside micelles, leaving the hydrophobic palm oil matrix to dominate the surface interface. Because bulk water is suppressed in this sample, Sample C possess a vastly superior electrochemical window. The risk of water splitting (electrolysis) at lower potentials is minimized, making this specific formulation less vulnerable to gas evolution, internal cell pressure, and premature electrode corrosion. While the suppression of water maximizes chemical stability, it introduces a severe penalty for ion transport. NaCl cannot dissociate easily within pure hydrophobic oil due to its low dielectric constant. Without a continuous bulk water network to form low-resistance pathways, $Na^+$ and $Cl^-$ mobility will be limited. Ion transport in Sample C is heavily throttled by the viscous, long aliphatic chains (2922.25 and 2854.74 $cm^{-1}$) of the oil matrix, which increases the internal resistance of the liquid cell. The carbonyl peak centers exactly at 1743.71 $cm^{-1}$. The lack of a downward shift confirms that the $Na^+$ ions are not actively coordinating with the bulk ester groups. Instead, the salt remains localized with the trace water phase inside isolated pockets within the oil matrix.

The FTIR spectrum for sample D, as seen in figure 4, represents a heavily oil-dominated system where water has been significantly restricted, well-emulsified, or mostly excluded from the surface layer during measurement. The Spectral analysis and functional groups for sample is seen in table 6

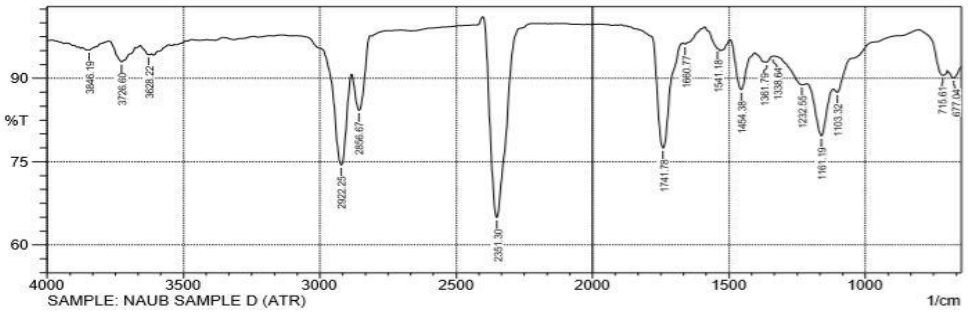


Figure 4: FTIR Spectra for Sample D

**Table 6: Spectral Analysis and Functional Groups for Sample D**

| Wavenumber ($cm^{-1}$) | Functional Group Assignment | Chemical Significance in Battery Application |
|---|---|---|
| 3846.19, 3726.60, 3628.22 | Weak, isolated free O–H stretching | Indicates trace, unbonded moisture pockets. The lack of a broad 3400 $cm^{-1}$ band proves there is no free bulk water layer. |
| 2922.25 & 2856.67 | Highly intense asymmetric and symmetric C–H stretching | Confirms the hydrophobic triglyceride core of the red palm oil remains robustly intact and dominates the mixture. |
| 2351.30 | Very deep, sharp peak from environmental atmospheric $CO_2$ | Indicates standard ambient background gas interference during testing. |
| 1741.78 | Deep, sharp C=O (Carbonyl) stretching | Confirms pristine ester bonds of the triglyceride host. Its baseline position indicates minimal direct coordination with the hydrated salt ions. |
| 1660.77 | C=C stretching of alkene groups | Represents the natural unsaturated fatty acids (oleic/linoleic components) inherent to red palm oil. |
| 1541.18 | Weak asymmetric carboxylate stretch | Traces of localized ion coordination or minimal breakdown at the interfacial boundary. |
| 1454.38, 1361.79, 1338.64 | Aliphatic C–H bending vibrations | Validates physical and mechanical backbone stability within the lipid fatty acid chains. |
| 1232.55 & 1161.19 & 1103.32 | Clean, distinct C–O stretching footprint | Fingerprint region confirming that the core glycerol-fatty acid ester linkages are fully preserved. |
| 715.61 & 677.04 | Aliphatic $CH_2$\rocking and skeletal variations | Confirms long-chain hydrocarbon integrity, which dictates the high viscosity of this liquid blend. |

The most critical feature of Sample D is the suppression of the bulk hydrogen-bonded water band (usually spanning broadly from 3200 to 3500 $cm^{-1}$). Instead, we only see weak, sharp peaks above 3600 $cm^{-1}$. This indicates that Sample D is heavily oil-dominated. The distilled water phase containing the dissolved KCl is likely entirely encapsulated deep within the hydrophobic oil matrix (water-in-oil micelle formation), shielding the water from dominating the ATR crystal contact surface. Because bulk free water is minimized at the surface, Sample D will present a vastly superior electrochemical stability window compared to highly aqueous variations like Sample B. The risk of the water-splitting reaction (electrolysis) is localized and throttled, allowing the liquid battery candidate to withstand higher charging potentials without immediate gas evolution ($H_2/O_2$), swelling, or premature electrode corrosion. While the oil preservation maximizes chemical and physical stability, it imposes severe limitations on battery performance. KCl requires a highly polar environment to dissociate into mobile $K^+$ and $Cl^-$ ions. Because the hydrophobic triglyceride environment dominates (shown by the massive 2922 and 1741 $cm^{-1}$ peaks), the ions face high transport resistance. The ion flux will be significantly hindered by the macro-viscosity of the long aliphatic chains, leading to high internal cell resistance. The carbonyl ester peak centers neatly at 1741.78 $cm^{-1}$. The lack of a distinct downward shift (like the 1737 $cm^{-1}$ shift observed in Sample A) proves that the potassium ions are mostly staying within their micro-aqueous domains rather than forming a tightly coordinated chelate network with the bulk oil's carbonyl groups.

The FTIR spectrum for Sample E, as seen in figure 5, reveals an identical formulation signature to Sample K. It successfully maps the co-existence of both the hydrophobic red palm oil matrix and the aqueous KCl electrolyte phase in a stable hybrid liquid matrix setup. The Spectral analysis and functional groups for this sample is seen in table 7

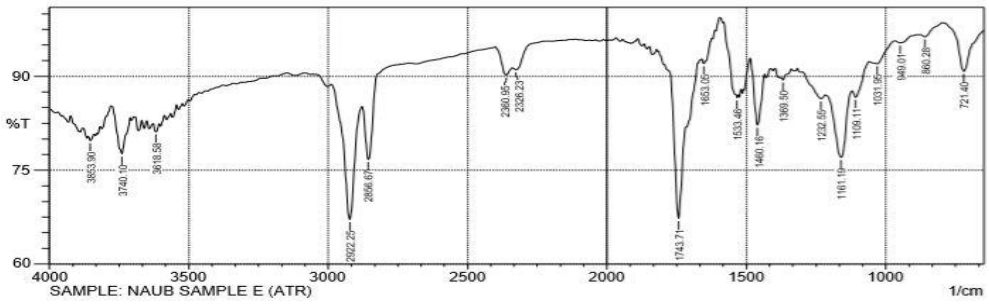


Figure 5: FTIR Spectra for Sample E

**Table 7: Spectral Analysis and Functional Groups for Sample E**

| Wavenumber ($cm^{-1}$) | Functional Group Assignment | Chemical Significance in Battery Application |
|---|---|---|
| 3853.90, 3740.10, 3618.58 | Sharp, distinct free O–H stretching | Proves the presence of active, unbonded water molecules acting as the dissolving medium for KCl salt. |
| 2922.25 & 2856.67 | Deep asymmetric and symmetric C–H stretching | Confirms that the long aliphatic hydrocarbon chains of the palm oil triglycerides remain fully intact and robust. |
| 2360.95 & 2326.23 | Doublet from environmental atmospheric $CO_2$ | Standard ambient background reading during testing. |
| 1743.71 | Highly intense, sharp C=O (Carbonyl) stretching | Confirms pristine triglyceride ester linkages. This provides core dipole-ion interaction potential. |
| 1653.05 | H–O–H water bending / C=C alkene stretching | Overlapping region showing water deformation and natural unsaturated fatty acid chains. |
| 1533.46 | Interfacial carboxylate complexation band | Points to localized ion coordination bridging the organic oil phase with the aqueous salt phase. |
| 1460.16 & 1369.50 | Aliphatic C–H bending vibrations | Validates the physical backbone stability within the lipid matrix. |
| 1232.55, 1161.19, 1109.11, 1031.95 | Multi-peaked C–O stretching profile | Fingerprint framework verifying that the baseline ester-glycerol skeleton has not broken down. |

| Wavenumber ($cm^{-1}$) | Functional Group Assignment | Chemical Significance in Battery Application |
|---|---|---|
| 949.01 & 860.28 | Out-of-plane C=C–H alkene variations | Represents unsaturated fatty acids (oleic/linoleic acids) present in red palm oil. |
| 721.40 | Aliphatic $CH_2$/ rocking vibration | Verifies long-chain structure, which dictates macro-fluid viscosity and limits rapid ion migration. |

The defining hallmark of Sample E is the balance between the intense organic peaks (2922.25 and 1743.71 $cm^{-1}$) and the clean water peaks (3800 - 3600 $cm^{-1}$). In a liquid battery configuration, this represents a successfully engineered emulsion. The oil does not isolate or reject the aqueous solution; instead, the two matrices physically weave together to yield an electrolyte system that offers both high fluid stability and consistent local ion distribution. Pure vegetable oils suffer from notoriously poor ion transport due to low dielectric capabilities. By keeping the free water phase visible (sharp O - H peaks), the KCl salt successfully dissociates into mobile $K^+$ and $Cl^-$. Water acts as a low-resistance fluid microchannel to maximize initial ionic conductivity, while the surrounding viscous palm oil works to cushion the system and prevent quick water evaporation. The emergence of the peak at 1533.46 $cm^{-1}$ is chemically highly valuable. This band signifies a carboxylate coordination mechanism. This suggests that a subset of dissolved potassium ($K^+$) ions is interacting at the boundary layer with the oxygen species of the palm oil triglycerides or trace free fatty acids, stabilizing the emulsion interface and creating a unified ion-conducting pathway. Because this hybrid matrix explicitly holds open water molecules, the operational voltage ceiling of the liquid-matrix battery cell remains thermodynamically limited. To circumvent water electrolysis, which triggers gas evolution ($H_2$ and $O_2$), internal pressure spikes, and electrode delamination, the cell charging voltage must be rigidly controlled below 1.23V.

The FTIR spectrum for Sample F, as seen in figure 6, represents another iteration of the red palm oil mixed with a potassium chloride (KCl) and distilled water electrolyte for liquid-matrix battery applications matches closely with Samples K and E, confirming high structural reproducibility in this specific hybrid emulsion series. The Spectral analysis and functional groups for this sample is seen in table 8

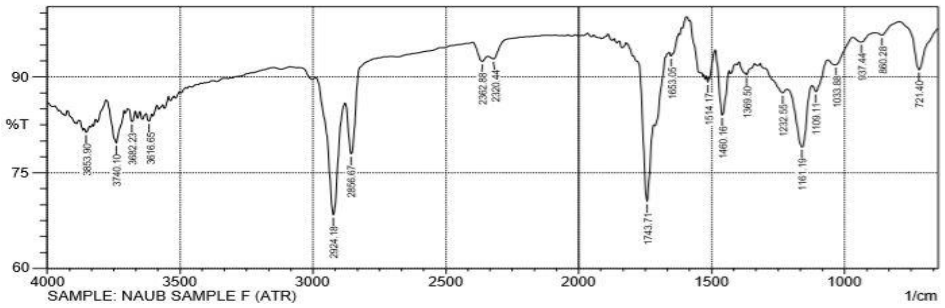

Figure 6: FTIR Spectra for Sample F

**Table 8: Spectral Analysis and Functional Groups for Sample F**

| Wavenumber ($cm^{-1}$) | Functional Group Assignment | Chemical Significance in Battery Application |
|---|---|---|
| 3853.90, 3740.10, 3682.23, 3616.65 | Sharp, multi-peaked free O–H stretching | Verifies active, unbonded water molecules that act as the primary polar vehicle to dissolve and dissociate the KCl salt. |
| 2924.18 & 2856.67 | Highly intense asymmetric and symmetric C–H stretching | Proves that the long, hydrophobic aliphatic hydrocarbon chains of the palm oil triglycerides remain fully intact. |
| 2362.88 & 2320.44 | Doublet from environmental atmospheric $CO_2$ | Standard ambient background gas reading during testing. |
| 1743.71 | Highly sharp, intense C=O (Carbonyl) stretching | Confirms pristine triglyceride ester linkages. It indicates that the bulk oil has not undergone complete destructive breakdown. |
| 1653.05 | H–O–H water bending / C=C alkene stretching | Overlapping region capturing the natural unsaturated fatty acid groups of the oil alongside water molecule deformations. |
| 1514.17 | Shifted carboxylate coordination band | Indicates localized ion-dipole or chemical interaction balancing the boundary between the oil and aqueous phases. |
| 1460.16 & 1369.50 | Aliphatic C–H bending vibrations | Validates the physical and structural stability of the underlying fatty acid alkane chains. |
| 1232.55, 1161.19, 1109.11, 1033.88 | Multi-peaked C–O stretching profile | Fingerprint framework verifying that the baseline ester-glycerol structural skeleton is fully preserved. |
| 937.44 & 860.28 | Out-of-plane C=C–H alkene variations | Represents unsaturated fatty acid configurations (like oleic or linoleic components) in the oil. |
| 721.40 | Aliphatic $CH_2$\rocking vibration | Confirms long-chain hydrocarbon integrity, contributing to the internal fluid viscosity. |

Sample F strongly reinforces the structural data seen in Samples K and E. The highly defined ester carbonyl peak at 1743.71 $cm^{-1}$ and the sharp aliphatic peaks (2924.18 and 2856.67 $cm^{-1}$) demonstrate that adding an aqueous salt electrolyte does not chemically destroy or rapidly hydrolyze the bulk triglyceride structure. Instead, a clean, multi-phase hybrid liquid matrix is successfully established. Because pure red palm oil has an incredibly low dielectric constant, it cannot effectively dissolve and separate solid KCl crystal networks on its own. The presence of the water peaks in the 3800 - 3600 $cm^{-1}$ region provides the highly polar environment required to fully dissolve KCl into mobile potassium ($K^+$) and chloride ($Cl^-$) ions. Water forms the continuous ionic transport pathways within the mixture, while the high viscosity of the surrounding oil matrix helps trap the moisture and lower its volatile evaporation rate. A minor yet highly informative variance in Sample F is the downward migration of the interfacial carboxylate/complexation band to

1514.17 $cm^{-1}$ (compared to 1533 $cm^{-1}$ in Samples K and E). This shift implies a slightly tighter or structurally unique coordination state between the potassium ($K^+$) ions and the local polar oxygen sites at the boundary where the water droplets interface with the bulk oil matrix. Since free water molecules are clearly mapped across the surface interface, the electrochemical window of Sample F will face strict thermodynamic limitations. To prevent water splitting (electrolysis) from generating gas ($H_2$ and $O_2$), which would cause immediate battery swelling and cell resistance spikes, the operating potential must be carefully regulated below 1.23 V.

The FTIR spectrum for Sample G, as seen in figure 7, represents a red palm oil mixture with NaCl and distilled water for a liquid-matrix battery application. This sample provides crucial new chemical information. It shows the emergence of a highly distinct secondary carbonyl signature at 1712.85 $cm^{-1}$, indicating that this specific formulation has undergone partial hydrolysis or a unique structural rearrangement under the influence of the aqueous NaCl electrolyte. The Spectral analysis and functional groups for this sample is seen in table 9

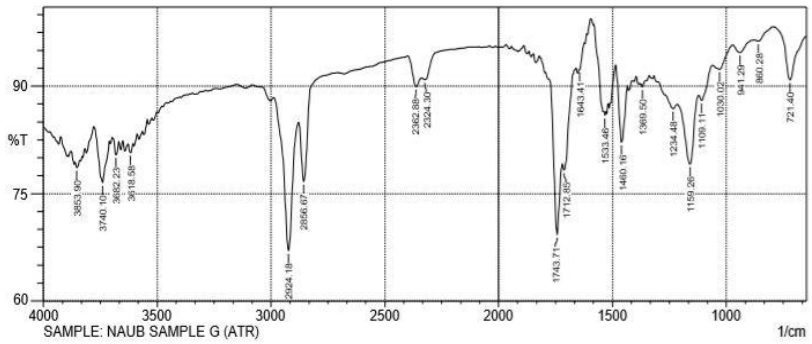


Figure 7: FTIR Spectra for Sample G

**Table 9: Spectral Analysis and Functional Groups for Sample G**

| Wavenumber ($cm^{-1}$) | Functional Group Assignment | Chemical Significance in Battery Application |
|---|---|---|
| 3853.90 to 3618.58 | Sharp, multi-peaked free O–H stretching | Confirms the presence of unbonded water molecules acting as the dissolving vehicle for the NaCl salt. |
| 2924.18 & 2856.67 | Strong asymmetric & symmetric C–H stretching | Proves that the long hydrophobic hydrocarbon tails of the triglycerides remain largely intact. |
| 2362.88 & 2324.30 | Doublet from environmental atmospheric $CO_2$ | Standard ambient background noise reading during testing. |
| 1743.71 | Highly sharp, intense C=O (Carbonyl) stretching | Represents the baseline triglyceride ester bonds from the preserved palm oil framework. |
| 1712.85 | Free Fatty Acid (FFA) C=O stretching / Hydrolysis shoulder | Critical Indicator: Confirms partial cleavage of triglyceride ester bonds into free carboxylic acids due to water interaction. |
| 1643.41 | H–O–H bending / C=C alkene stretching | Captures water molecule deformation overlapping with natural unsaturation in the oil. |
| 1533.46 | Carboxylate salt or shifted coordination band | Represents localized chemical complexation where $Na^+$ ions interact with cleaved or shifted fatty acid oxygen sites. |
| 1460.16 & 1369.50 | Aliphatic C–H bending vibrations | Validates the physical and structural backbone stability of the underlying alkane chains. |
| 1234.48, 1159.26, 1109.11, 1030.02 | Clean, distinct C–O stretching footprint | Represents the ester and glycerol skeletal linkages of the oil matrix. |
| 721.40 | Aliphatic $CH_2$\ rocking vibration | Verifies long-chain structure, contributing to the internal fluid viscosity of the liquid cell. |

The standout feature of Sample G is the sharp secondary peak at 1712.85 $cm^{-1}$ sitting directly next to the primary ester peak (1743.71 $cm^{-1}$). In vegetable oils, a peak around 1710 - 1712 $cm^{-1}$ signifies free fatty acids (FFAs) containing unesterified protonated carboxylic acid groups (COOH). This means that mixing the red palm oil with NaCl and distilled water in this specific ratio or duration has initiated partial hydrolysis. The water splitted some of the triglyceride molecules into free fatty acids and diglycerides/glycerol. From a battery performance standpoint, partial hydrolysis is a double-edged sword. Free fatty acids are much more polar than intact triglycerides. The free -COOH groups can interact strongly with mobile Na ions, acting as localized ion-coordinating sites that improve salt dissociation and potentially boost interfacial ionic conductivity. The presence of free fatty acids increases the chemical acidity of the liquid matrix. This can accelerate chemical corrosion at the battery electrodes (especially if using standard metallic anodes like zinc, aluminum, or sodium metal), leading to premature cell degradation. Like the other stable hybrid emulsions, Sample G preserves its sharp water peaks between 3800 and 3600 $cm^{-1}$ while avoiding a massive bulk water valley at 3400 $cm^{-1}$. This indicates that the water phase remains controlled and well-emulsified. The water allows the NaCl to dissociate cleanly into active charge carriers, while the oil matrix acts as a viscous shield to limit evaporation. Because free water molecules and newly formed free fatty acid groups are co-present in the liquid system, the electrochemical breakdown limits are highly sensitive. To avoid rapid water electrolysis and gas generation (H2/O2), the cell must be operated within a strict voltage window under 1.23V.

The FTIR spectrum for Sample H, as seen in figure 8, analysed using the KBr pellet method, represents a red palm oil mixture with NaCl and a distilled water electrolyte for liquid-matrix battery applications. The Spectral analysis and functional groups for this sample is seen in table 10.

This spectrum shares striking similarities with Sample J. The use of the KBr pellet preparation technique has resulted in the heavy dominance of the aqueous phase, leading to a near-total flattening or masking of the oil's primary organic signatures.

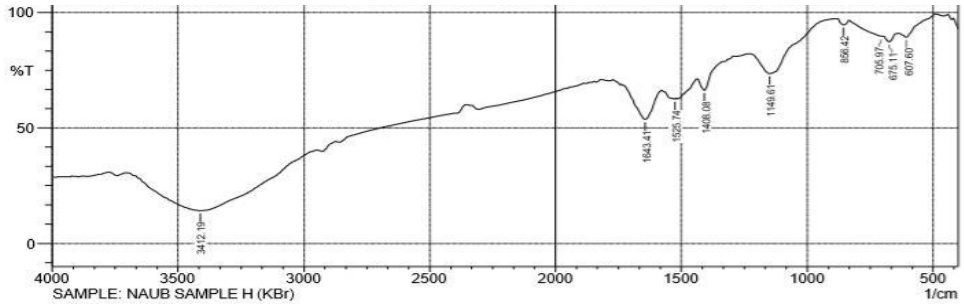


Figure 8: FTIR Spectra for Sample H

**Table 10: Spectral Analysis and Functional Groups for Sample H**

| Wavenumber ($cm^{-1}$) | Functional Group Assignment | Chemical Significance in Battery Application |
|---|---|---|
| 3412.19 | Massive, broad hydrogen-bonded O–H stretching valley | Confirms a heavily dominant bulk water matrix wrapping completely around the active ionic species. |
| 1643.41 | Deep, sharp H–O–H bending vibration | Further reinforces the dominant presence of free, uncoordinated water acting as the salt solvent. |
| 1525.74 | Strong carboxylate salt formation / saponification product | Indicates a major structural shift where fatty acid groups are heavily complexed with $Na^+$ ions at the interface. |
| 1408.08 | Aliphatic C–H bending or localized carbonate traces | Structural fingerprint of the remaining carbon skeletal remnants. |
| 1149.61 | Weakened C–O single bond stretching | Traces of the residual glycerol-fatty acid backbone heavily masked by the water phase. |
| 856.42 to 607.60 | Multi-peaked finger-print / Na-Cl aqueous skeletal rocking | Reflects the highly altered and fully dissolved inorganic salt environment. |

The defining visual and chemical trait of Sample H is the massive, deep absorption valley centered at 3412.19 $cm^{-1}$ alongside the complete absence of the sharp triglyceride ester peak (typically at 1741 $cm^{-1}$) and the aliphatic C–H chains (2922 $cm^{-1}$). This indicates that the KBr technique has primarily captured the bulk aqueous electrolyte layer. The oil phase has either undergone severe localized hydrolysis (breaking into glycerol and free acids) or has physically separated, leaving the water to completely saturate the pellet window. Because bulk water dominates this configuration completely, the NaCl salt is perfectly and thoroughly dissociated into free sodium ions and chloride ions. In an electrochemical cell, this specific configuration provides the least internal transport resistance. The charge-carrying ions do not have to fight through the macro-viscosity of dense organic oil matrices; they can drift freely through an open, low-viscosity aqueous network. The sharp peak at 1525.74 $cm^{-1}$ represents a highly pronounced carboxylate salt state. This confirms that at the boundaries where the water phase meets any trace lipid fractions, a strong saponification-like or ion-chelation reaction has occurred. The Na+ are highly reactive with the broken-down or shifted polar segments of the oil matrix, binding tightly to form structural interfacial bridges. While Sample H will yield exceptional initial ionic conductivity due to its open aqueous channels, it suffers from severe thermodynamic limitations; The prominent 3412.19 $cm^{-1}$ and 1643.41 $cm^{-1}$ water peaks mean this liquid matrix will undergo rapid water splitting (electrolysis) if the cell charging voltage exceeds 1.23V. Operating past this limit will cause rapid gas generation (H2 and O2), causing severe pressure build-up, cell gassing, and accelerated degradation of the battery electrodes.

The Fourier Transform Infrared (FTIR) spectrum for Sample I as seen in figure 9, represents the chemical structure of red palm oil mixed with a sodium chloride (NaCl) electrolyte tailored for battery applications. The Spectral analysis and functional groups for this sample is seen in table 11.

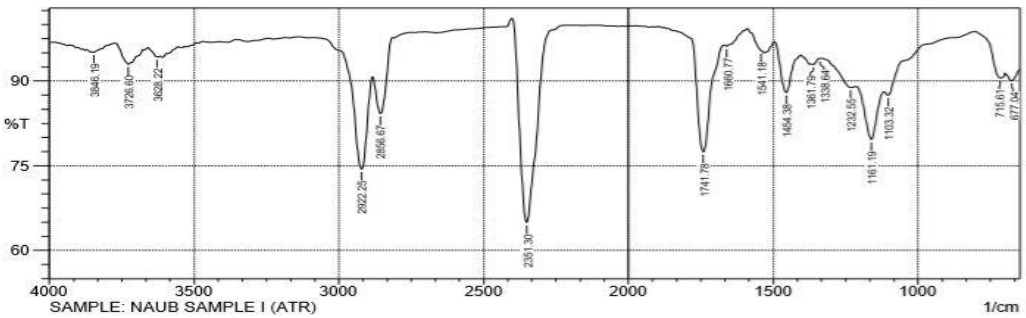


Figure 9: FTIR Spectra for Sample I

**Table 11: Spectral Analysis and Functional Groups for Sample I**

| Wavenumber ($cm^{-1}$) | Functional Group Assignment | Chemical Significance in Battery Application |
|---|---|---|
| 2922.25 & 2856.67 | Asymmetric and symmetric C–H stretching (aliphatic -$CH_2$ / -$CH_3$) | Confirms the hydrophobic hydrocarbon backbone of the triglycerides in the red palm oil. |
| 2351.30 | Sharp, deep peak associated with environmental atmospheric $CO_2$ or complexed species | Indicates either background atmospheric carbon dioxide or a structural change arising during mixture formulation. |
| 1741.78 | Intense C=O (Carbonyl) stretching of ester groups | Represents the central triglyceride ester bonds. These oxygen atoms provide coordination sites for mobile $Na^+$ ions. |
| 1660.77 | C=C stretching vibration of cis-alkenes | Indicates the presence of unsaturated fatty acids (e.g., oleic and linoleic acids) inherent to palm oil. |
| 1454.38 & 1361.79 | Aliphatic C–H bending / scissoring of alkanes | Confirms structural stability and bending vibrations within the fatty acid lipid matrix. |
| 1161.19 & 1103.32 | C–O stretching vibration of ester groups | Represents the fingerprint of the glycerol-fatty acid bridge linkages. |

The highly sharp, distinct carbonyl peak at 1741.78 $cm^{-1}$ highlights that the triglyceride structure remains stable even after introducing the NaCl electrolyte. In green battery design, the lone pairs of electrons on these oxygen atoms coordinates loosely with the $Na^+$ cations, helping dissolve the salt and enabling ionic mobility. Safe, non-toxic NaCl functions as the salt source to provide charging carriers ($Na^+$ and $Cl^-$). The shift or preservation of the ester fingerprint regions indicates a stable liquid or gel polymer electrolyte environment where the ion-dipole interaction drives sodium-ion conduction. The minimal, weakly broad signal in the 3600 - 3800 $cm^{-1}$ region represents free -OH stretching. Its remarkably low profile reveals that the mix preserves high hydrophobic integrity, reducing water-induced side reactions or cell corrosion inside a battery enclosure

The FTIR spectrum for Sample J, as seen in figure 10, represents red palm oil mixed with potassium chloride (KCl) and distilled water, prepared using the KBr pellet method for a liquid-matrix battery application. Compared to Sample I, this spectrum shows drastic flattening and structural alteration, indicating severe degradation, hydrolysis, or scattering effects caused by the addition of water. The Spectral analysis and functional groups for this sample is seen in table 12.

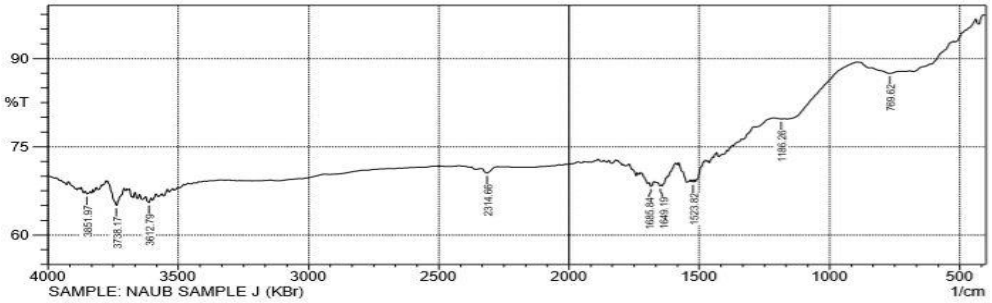


Figure 10: FTIR Spectra for Sample J

**Table 12: Spectral Analysis and Functional Groups for Sample J**

| Wavenumber ($cm^{-1}$) | Functional Group Assignment | Chemical Significance in Battery Application |
|---|---|---|
| 3851.97 to 3612.79 | Sharp, multi-peaked free O–H stretching | Confirms the presence of uncoordinated or bound water molecules from the distilled water component. |
| 2314.66 | Weak environmental $CO_2$ or shallow background noise | Minor atmospheric presence; significantly less prominent than in Sample I. |
| 1685.84 & 1649.19 | H–O–H bending of water overlapping with shifted C=O/C=C bonds | Indicates a strong presence of free water. The broadness suggests water molecules are splitting or interacting with the organic matrix. |
| 1523.82 | Altered organic structure / carboxylate salt formation | Suggests saponification or degradation products. The original 1741 $cm^{-1}$ ester peak has collapsed completely. |
| 1186.26 | Weak C–O single bond stretching | Traces of the remaining ester/glycerol skeleton, heavily degraded or masked by the aqueous phase. |
| 769.62 | Out-of-plane C–H or K-Cl / aqueous skeletal rocking | Reflects the highly altered local environment of the liquid mixture. |

The defining feature of this spectrum is the complete loss of the sharp triglyceride ester peak (1741 $cm^{-1}$) and the aliphatic chains (2922 $cm^{-1}$). Mixing red palm oil with water and KCl has likely triggered a hydrolysis reaction, breaking down triglycerides into free fatty acids and glycerol, or causing massive phase separation where the oil phase was excluded from this specific KBr testing window. Distilled water successfully dissolves KCl to produce highly mobile charge carriers ($K^+$ and $Cl^-$), which exponentially boosts initial ionic conductivity compared to pure oil. However, the presence of water creates a highly corrosive and electrochemically unstable environment for battery electrodes. Water introduces the water-splitting reaction. This limits the liquid battery's operating voltage to a theoretical maximum of 1.23V. Exceeding this voltage will cause gas evolution ($H_2$ and $O_2$), leading to cell swelling and failure.

The FTIR spectrum for Sample K, as seen figure 11, analysed using Attenuated Total Reflection (ATR), provides a much clearer and more successful representation of the red palm oil, KCl, and distilled water mixture. Unlike Sample J (which suffered from poor KBr pellet resolution), the ATR technique successfully captures the co-existence of both the

hydrophobic oil matrix and the aqueous electrolyte phase without losing the oil's core chemical structure. The Spectral analysis and functional groups for this sample is seen in table 13

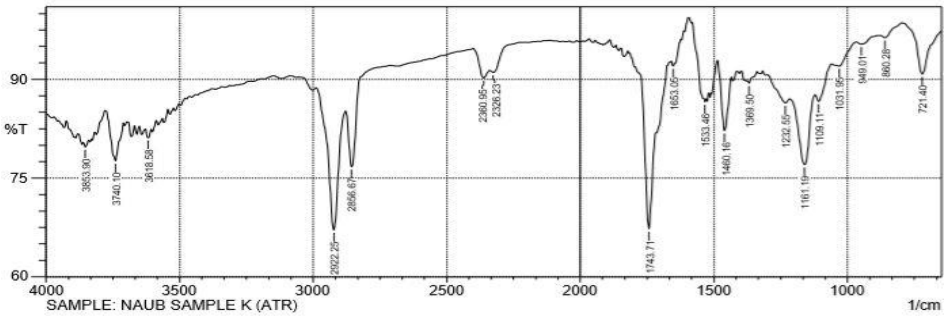


Figure 11: FTIR Spectra for Sample K

**Table 13: Spectral Analysis and Functional Groups for Sample K**

| Wavenumber ($cm^{-1}$) | Functional Group Assignment | Chemical Significance in Battery Application |
|---|---|---|
| 3853.90, 3740.10, 3618.58 | Sharp, distinct O–H stretching vibrations | Confirms the presence of free and weakly bound water molecules from the distilled water component, which dissolves the KCl salt. |
| 2922.25 & 2856.67 | Strong asymmetric and symmetric C–H stretching | Proves that the long-chain aliphatic hydrocarbon chains of the red palm oil triglycerides are fully intact and preserved. |
| 2360.95 & 2326.23 | Doublet from environmental atmospheric $CO_2$ | Standard ambient background reading during testing. |
| 1743.71 | Highly intense, sharp C=O (Carbonyl) stretching | Confirms the triglyceride ester bonds are fully intact. This serves as the primary coordination site for ion-dipole interactions. |
| 1653.05 | C=C alkene stretch / H–O–H water bending | Represents the unsaturated fatty acids in the oil overlapping with the bending vibration of water. |
| 1533.46 | Shifted carboxylate / local coordination peak | Indicates a localized interaction between the dissolved salt ions ($K^+/Cl^-$), water molecules, and the oil matrix. |
| 1460.16 & 1369.50 | Aliphatic C–H bending (scissoring/rocking) | Confirms the structural stability of the underlying alkane fatty acid chains. |
| 1161.19, 1109.11, 1031.95 | Fingerprint C–O stretching of ester groups | Validates that the core glycerol-fatty acid ester linkages have not undergone total destructive hydrolysis. |
| 721.40 | Aliphatic $–(CH_2)_n–$ rocking vibration | Confirms long-chain hydrocarbon integrity, contributing to the fluid matrix's viscosity. |

The most critical finding in Sample K is that the oil matrix has not degraded. The appearance of the intense ester peak at 1743.71 $cm^{-1}$ alongside the sharp aliphatic peaks (2922.25 and 2856.67 $cm^{-1}$) confirms that the triglycerides remain robust. This proves that red palm oil can physically co-exist with an aqueous KCl solution as a liquid matrix, likely forming a temporary or stable emulsion rather than undergoing immediate destructive hydrolysis. The presence of water is clearly visible in the 3800–3600 $cm^{-1}$ region. In a pure oil battery, low salt solubility severely limits ion transport. By introducing distilled water, the KCl salt fully dissociates into mobile potassium (K+) and chloride (Cl-) ions. Water serves as a high-dielectric transport medium, while the surrounding oil matrix acts as a thick, viscous damper that can slow down evaporation and control ion diffusion rates. The sharp peak appearing at 1533.46 $cm^{-1}$ is highly significant. This frequency typically points to a carboxylate salt or a strongly shifted carbonyl environment. This suggests that some K+ are interacting directly with the oxygen atoms of the oil or a small fraction of free fatty acids, creating a complexed network that bridges the aqueous electrolyte phase and the organic oil phase. While the water phase ensures excellent initial ionic conductivity, it introduces a strict thermodynamic limit. The operating voltage of this liquid matrix cell must be kept below 1.23V to prevent water electrolysis (gas evolution).

The FTIR spectrum for Sample L, as seen in figure 12, analyzed via Attenuated Total Reflection (ATR), represents a red palm oil mixture with a potassium chloride (KCl) and distilled water electrolyte for a liquid-matrix battery application. This sample provides critical structural data matching the degradation behaviour seen in the NaCl series (Sample G). It reveals a highly distinct secondary carbonyl signature at 1712.85 $cm^{-1}$, indicating that this specific KCl formulation has undergone partial matrix hydrolysis or chemical rearrangement. The Spectral analysis and functional groups for this sample is seen in table 14.

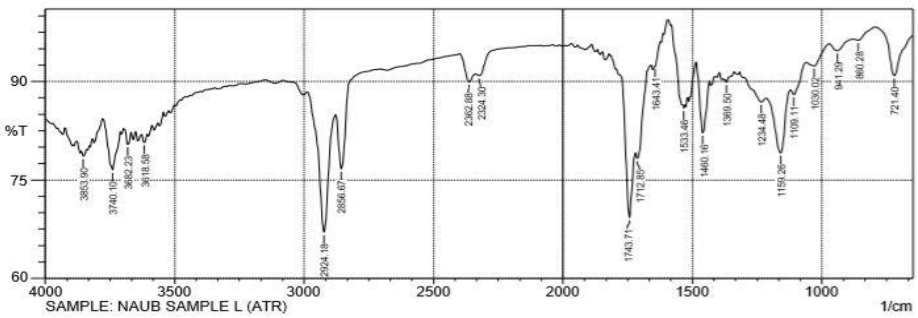


Figure 12: FTIR Spectra for Sample L

**Table 14: Spectral Analysis and Functional Groups for Sample L**

| Wavenumber ($cm^{-1}$) | Functional Group Assignment | Chemical Significance in Battery Application |
|---|---|---|
| 3853.90 to 3618.58 | Sharp, multi-peaked free O–H stretching | Confirms the presence of unbonded water molecules acting as the continuous medium to dissolve and dissociate the KCl salt. |
| 2924.18 & 2856.67 | Strong asymmetric & symmetric C–H stretching | Proves that the long, hydrophobic aliphatic hydrocarbon chains of the triglycerides remain largely intact. |
| 2362.88 & 2324.30 | Doublet from environmental atmospheric $CO_2$ | Standard ambient background noise reading during testing. |
| 1743.71 | Highly sharp, intense C=O (Carbonyl) stretching | Represents the baseline triglyceride ester bonds from the preserved palm oil framework. |
| 1712.85 | Free Fatty Acid (FFA) C=O stretching / Hydrolysis shoulder | Critical Indicator: Confirms partial cleavage of triglyceride ester bonds into free carboxylic acids (-COOH) due to water interaction. |
| 1643.41 | H–O–H bending / C=C alkene stretching | Captures water molecule deformation overlapping with natural unsaturation in the oil. |
| 1533.46 | Carboxylate salt or shifted coordination band | Represents localized chemical complexation where $K^+$ interact with cleaved or shifted fatty acid oxygen sites. |
| 1460.16 & 1369.50 | Aliphatic C–H bending vibrations | Validates the physical and structural backbone stability of the underlying alkane chains. |
| 1234.48, 1159.26, 1109.11, 1030.02 | Clean, distinct C–O stretching footprint | Fingerprint framework verifying the ester and glycerol skeletal linkages of the oil matrix. |
| 721.40 | Aliphatic $CH_2$\ rocking vibration | Verifies long-chain structure, contributing to the internal fluid viscosity of the liquid cell. |

The defining feature of Sample L is the sharp secondary peak at 1712.85 $cm^{-1}$ located immediately adjacent to the primary ester carbonyl peak (1743.71 $cm^{-1}$). In plant-based lipid matrices, a peak in the 1710–1712 $cm^{-1}$ range signifies the presence of free fatty acids (FFAs) with protonated carboxylic acid groups. This proves that introducing the aqueous KCl electrolyte has initiated a partial hydrolysis reaction, breaking a fraction of the triglyceride molecules down into free fatty acids and lower glycerides. From an electrochemical engineering perspective, this partial structural breakdown has a dual effect; the generation of free fatty acids introduces highly polar -COOH channels into the hydrophobic lipid bulk, also it can actively coordinate with mobile potassium ions, acting as localized ion-conducting bridges that lower the desolvation energy at the oil-water interface. Free fatty acids introduce a weak acidic character to the liquid matrix. This acidity can aggressively attack metallic battery electrodes (such as zinc, aluminum, or magnesium anodes), generating unwanted passivating layers or structural corrosion that degrades the battery's lifespan. The retention of sharp water peaks between 3800 and 3600 $cm^{-1}$ (without the large bulk water valley at 3400 $cm^{-1}$) indicates a highly controlled micro-emulsion. The water domains allow the solid KCl crystals to fully dissociate into free charge carriers K+ and Cl-, ensuring reasonable ion transport, while the surrounding viscous oil acts as a physical barrier to restrict moisture evaporation. Because free water molecules and reactive free fatty acids are concurrently mapped across the interface, this liquid matrix faces strict thermodynamic voltage limitations. The cell operating potential must be meticulously regulated below 1.23V to prevent water splitting (electrolysis) from producing gaseous hydrogen and oxygen, which leads to immediate cell swelling and catastrophic internal resistance spikes

## CONCLUSION

In conclusion, the Attenuated Total Reflection (ATR-FTIR) monitoring revealed a notable coordinate bathochromic shift of the triglyceride ester carbonyl to 1737.92 $cm^{-1}$ uniquely in the NaCl system (Sample A), indicating direct cation chelation. Conversely, the KCl system maintained a baseline ester peak at 1743.71 $cm^{-1}$, indicating that larger $K^+$ ions remain confined within polar aqueous microchannels. Furthermore, critical boundaries were identified between water-overloaded systems displaying extensive hydrogen bonding (3394.83 $cm^{-1}$) and oil-encapsulated micellar networks. Spectroscopic evidence also uncovered an identical partial hydrolysis pathway for both salts (1712.85 $cm^{-1}$ free fatty acid shoulder), highlighting a key challenge for battery shelf-life. Finally, a comparison of methods showed that classical KBr pelletization causes phase displacement that obscures organic signatures, establishing ATR as the required technique for characterisation. These findings provide a framework for balancing ionic conductivity, voltage stability, and corrosion resistance in biomass-derived liquid batteries.

## REFERENCES

Alpha, M., U.E Uno., Isah, KU., Ahmadu U. (2019). Structural and Electrochemical Properties of AgxSnO1-x/G ($0.3 \leq \times \leq 0.4$) Composite Electrode. European Journal of Scientific Research,151, 479-488

Bard, A.J, G. Inzelt, F. Scholz, Electrochemical Dictionary, Springer-Verlag, Berlin Heidelberg, 2008 10.1007/978-3-540-74598-3

Bard, A.J., L.R. Faulkner, Electrochemical Methods Fundamentals and Applications, 2nd ed., John Wiley & Sons, New York, Chichester, Weinheim, Brisbane, Singapore, Toronto, 1981.

Bello, A., Fabiane, M., Momodu, D. Y., Khamlich, S., Dangbegnon, J., & Manyala, N. (2014) Functionalized graphene form as electrode for improved electrochemical storage. Journal of Solid State Electrochemistry, 18, 2359 https://doi.org/10.1007/s10008-014-2473-4

Borghols WJH, Wagemaker M, Lafont U. (2009). Size effects in the Li4+xTi5O12 spinel. Journal American Chemical Society, 131: 17786–17792 https://doi.org/10.1021/ja902423e

Chen, H. H., Peng, M., & Zhang, X. (2006). Modeling and simulation of electrochemical capacitors with carbon

nanotube electrodes. Journal of Applied Physics, 99(5) https://doi.org/10.1063/1.2173111

Chen, J., Wu, K., Li, W., Chen, K., Cao, D., & Luo, X. (2019). Synthesis of Al2O3/K2CO3-modified activated carbon derived from coconut husk by microwave-assisted method for high-performance supercapacitors. Ceramics International, 45(16), 20476-20486 https://doi.org/10.1016/j.ceramint.2019.07.011

Ejike, C. E. (2023). Oxidative stability of red palm oil from two oil palm varieties (Elaeis guineensis and Elaeis oleifera): Comparative effects of storage temperature and duration. African Journal of Food Science, 17(2), 45-52.

Nadeem, M., et al. (2023). Study of Ionic Interactions of Potassium in Organic Suspensions. Studia Universitatis Babes-Bolyai Chemia, 68(1), 59-74 https://doi.org/10.24193/subbchem.2023.1.05

Okonkwo, C. J., & Mensah, A. (2022). Physicochemical Properties of Crude Red Palm Oil for Industrial Applications. African Journal of Biotechnology, 21(4), 145-152.

Yusuf, B. A., et al. (2023). Antioxidant Synergetic Effects in Vegetable Oil-Based Dielectric Fluids. Industrial Crops and Products, 192, 116-125.